Supplementary Information

Diffuse Optical Ptychography

Mingwei He[1], Sujit K. Sahoo[2*], Chengyuan Xiao[1] and Cuong Dang[1*]

[1] School of Electrical and Electronic Engineering, Nanyang Technological University Singapore, 50 Nanyang Avenue, 639798, Singapore

[2] School of Electrical Sciences, Indian Institute of Technology Goa, Goa 403401, India

[*]Corresponding author, Email: hcdang@ntu.edu.sg, sujit@iitgoa.ac.in

Supplementary Figures:

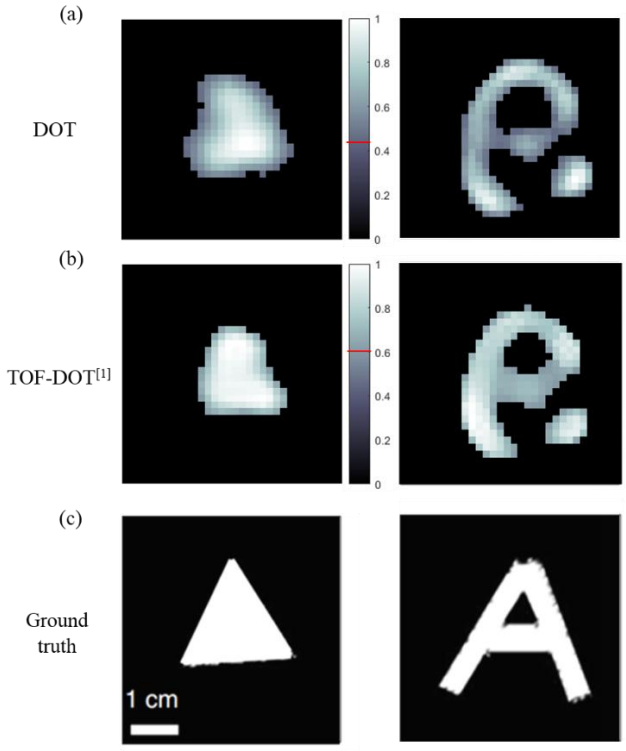

Figure S1. Experimental results with time-integrated measurements and time-resolved measurements after image enhancement. a) The DOT result with a single 2D image as input for reconstruction (45% thresholding). **b)** ToF-DOT result reconstructed with all temporal frames (60% threshold). The image contrast in these figures is boosted by thresholding, i.e. set all the pixels with intensity less than 45% (figure a) or 60% (figure b) to have intensity of zero. The original images (without contrast enhancement) are presented in Fig. 2. **c)** Ground truth. Figures a, b, c share the same scale bar as presented in figure c.

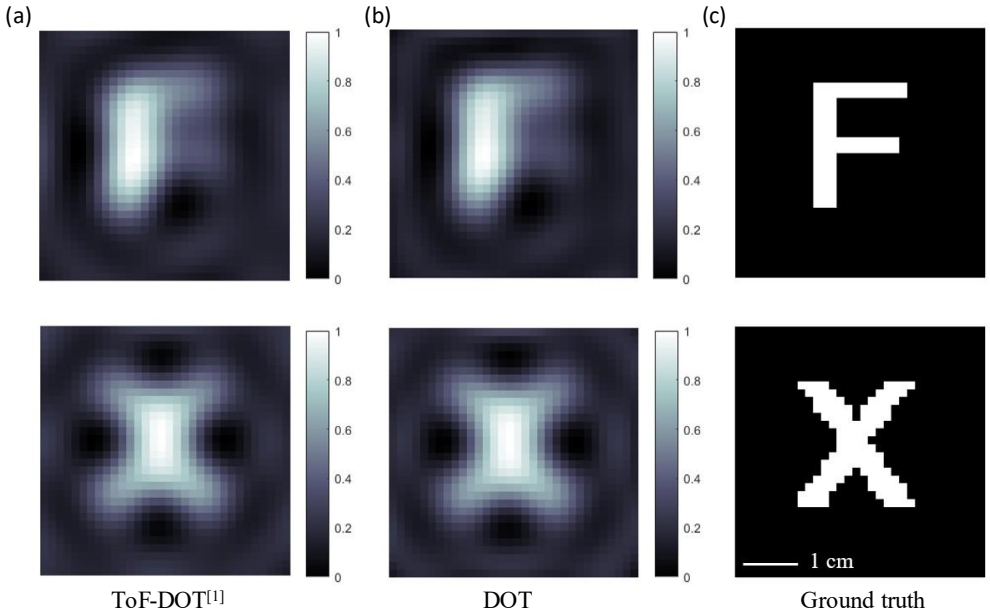

Figure S2. Simulation results with time-integrated measurements and time-resolved measurements. a) ToF-DOT result reconstructed with all temporal frames. **b)** The DOT result with a single 2D image as input for reconstruction. **c)** Ground truth. Figure a, b, c share the same scale bar as presented in figure c. The parameters are set to approximate Lyons' experiment[1].

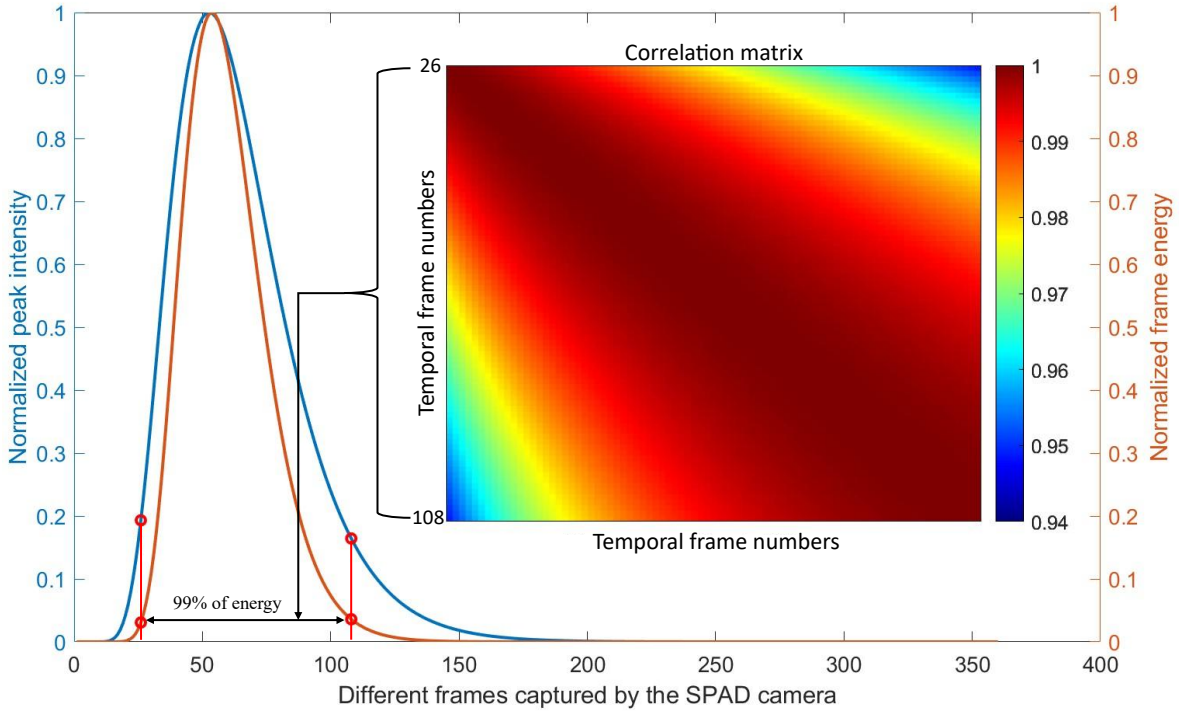

Figure S3. The intensity of SPAD camera-captured temporal images and their correlations. A heatmap is used to demonstrate the correlation among the temporal frames captured by a SPAD camera. Here, we only consider the frames that contribute 99% of the total energy. Their correlation coefficients consistently exceed 94.5%, highlighting the temporal similarities of images captured by SPAD camera. The scale bar for heatmap is from 0.94 to 1.

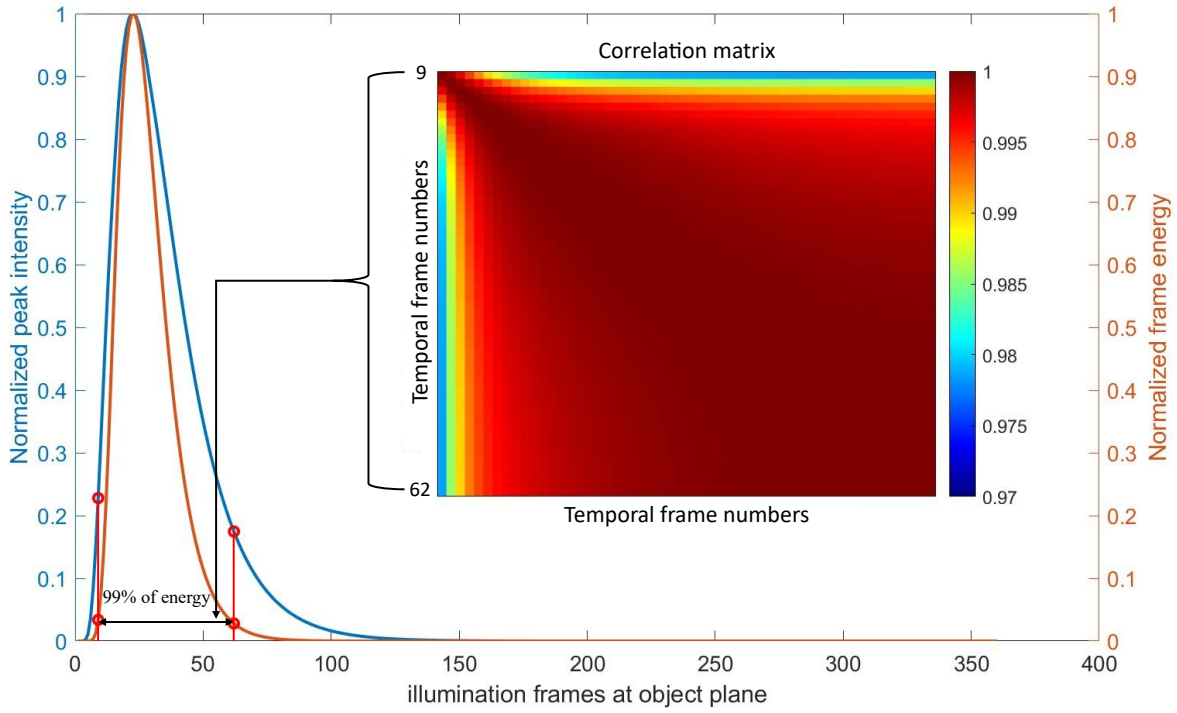

Figure S4. The intensity of temporal frames on the object plane and their correlations. A heatmap is used to demonstrate the correlation among the temporal frames captured by a SPAD camera. Here, we only consider the frames that contribute 99% of the total energy. Their correlation coefficients consistently exceed 97.5%, highlighting the similarity of the light illuminated on the object at different time frames. The scale bar for heatmap is from 0.97 to 1.

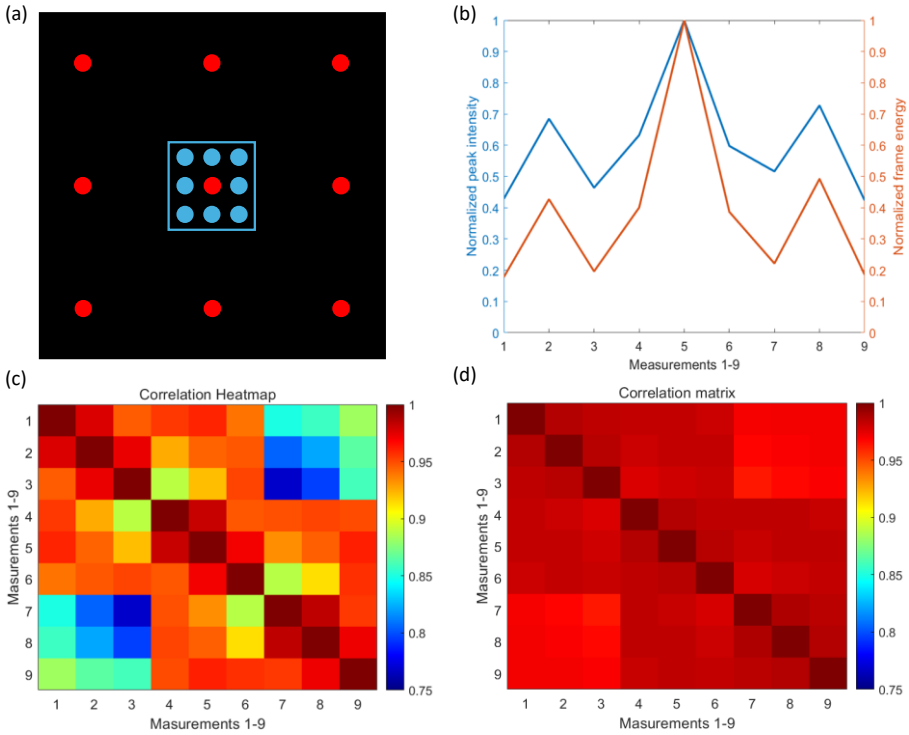

Figure S5. The intensity and correlation of captured images in DOP. a) Illumination points on the surface of the first diffusion block. The **b)** intensity of normal camera-captured images under 3x3 illumination points (red) and their **c)** correlations. **d)** The correlation matrix of 9 captured images corresponding to denser 3x3 illumination points at the center (blue square). The decrease of the distance between illumination points increases the correlation coefficients.

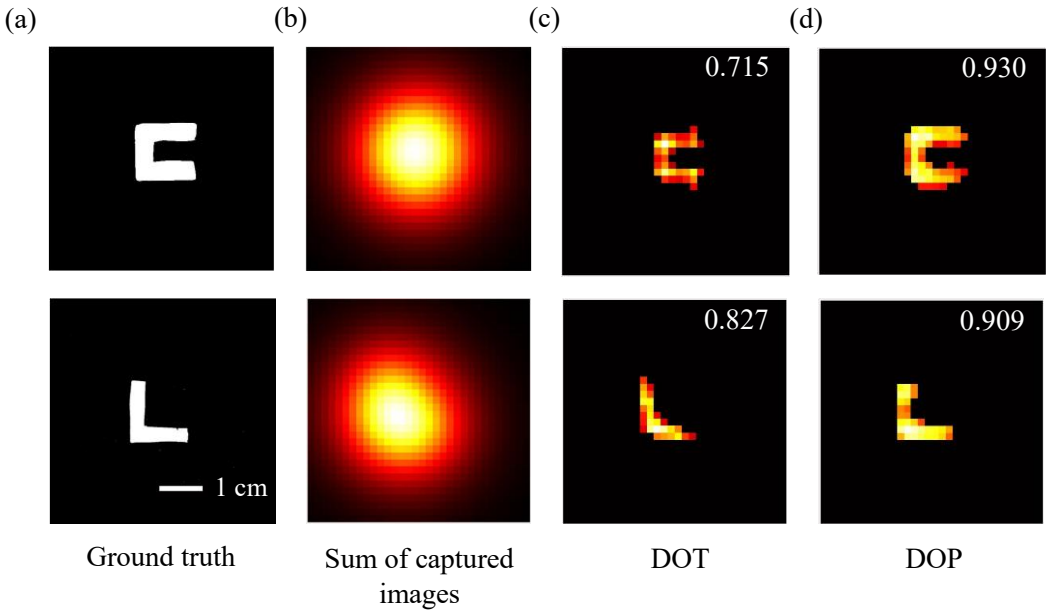

Figure S6. Additional DOT and DOP reconstruction results with diffusion calibration: a) Ground truth **b)** Sum of 9 camera captured images with different illumination point, which is the measurement for DOT. **c)** The DOT result with figure b as input for reconstruction **d)** DOP result with 9 images as input for reconstruction. They all have the same scale bar as presented in the figure a. The number at corner indicates the corresponding correlation coefficient relative to the ground truth.

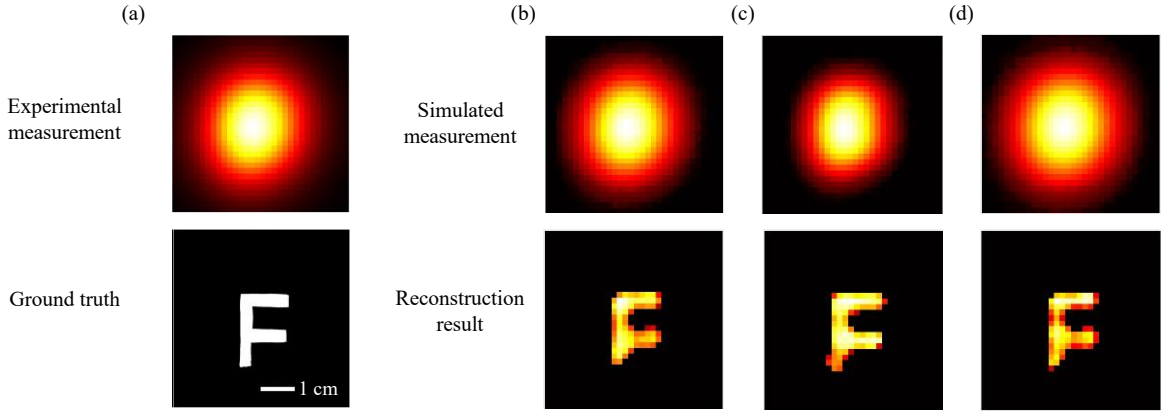

Figure S7. Simulation results in different unknown diffusive environments.: a) Ground truth and experimental measurement obtained by summing 9 captured images **b)** Simulation result under experimental conditions, replicating the optical properties of the experimental setup. **c)** Simulation result under a less diffusive environment. **d)** Simulation result under a more diffusive environment. Figure a, b, c, d share the same scale bar as presented in Figure a.

Note 1: Experimental Setup

The experimental setup is schematically illustrated in Fig. 1. A scanning mirror (KS1-Z9, Thorlabs) directs the laser beam to various locations on the diffusive slab, so that a continuous wave laser source (532nm) can illuminates the object hidden between two diffusive epoxy slabs. The laser power is relatively low (60 mW), so one can make a LED array to make the simpler and even more accurate scanning illumination. The hidden object is fabricated by cutting various shapes from black paper. The diffused light propagating through the object is captured by a CMOS camera (Neo 5.5 sCMOS, Andor. 2560 x 2160 with pixel size of 6.5 μm) placed on the other side of diffusive slabs. To identify the object region, we first perform a coarse scan using a 9×9 array across the entire input plane and calculate the corresponding measurement energy. Based on the energy

distribution from these 81 points, we define the region of interest. Subsequently, we conduct a finer scan in the region of interest using a 3×3, or 5×5 or 9×9 square array illumination and store the captured images for our DOP algorithm. To optimize computational efficiency, the images are cropped then downsampled to 32×32/64×64/96×96 resolution. The entire image acquisition process is fully automated, with both the camera and scanning mirror connected to a desktop computer. The camera will capture a new image once the scanning mirror switched to a new direction.

Compared to ToF-DOT, our DOP does not have an issue with timing jitter, but the position precision of illumination points on the first surface and their corresponding positions in camera's coordinates is very crucial in DOP. However, it can be done with careful alignment and calibration as pixel size in the experiment is relatively large, which are 1.68mm, 0.84mm, or 0.56mm for the resolution of 32x32, 64x64, or 96x96, respectively. Again, for diffusive media, it is not necessary to go to higher resolution image because of the smoothness of the diffused patterns.

The diffusive slabs used in this experiment consist of epoxy resin mixed with titanium oxide (TiO_2) powders (≥99% trace metals basis, Sigma-Aldrich) at a weight ratio of 1600:1. To calibrate the absorption, μ_a, and reduced scattering coefficients, μ_s', we fabricated a new slab of the same thickness using transparent clear epoxy, as the influence of titanium oxide powder on the absorption coefficient is negligible. After testing the slab with a uv-vis spectrophotometer, this slab had a reflectance of 10% and a transmittance of 84%, so the absorption coefficient was calculated to be $\mu_a = -\frac{\ln(1-A)}{Thickness} = -\frac{\ln(R+T)}{Thickness} = 0.039\ cm^{-1}$. Certainly the absorption of TiO_2 microspheres is negligible because of both its extremely low absorption coefficient at 532nm wavelength and its super small quantity. The reduced scattering coefficient, μ_s', can be obtained by fitting the time-integrated diffusion solution (Eq. S1) to the PSF measured by a CMOS camera[2].

With a pulsed laser point source illumination, the time-resolved diffusion solution can be expressed analytically as equation (S1) [3,4]:

$$PSF_{3D} = \phi(x,y,t) = \frac{c}{(4\pi Dct)^{3/2}} \exp\left(-\frac{x^2+y^2+d^2}{4Dct} - \mu_a ct\right) \qquad \text{(S1)}$$

where d, t is the observation depth and time, c denotes the speed of light in the scattering medium, and $D = \frac{1}{3(\mu_a+\mu_s')}$ is the diffusion coefficient. Here, we assume that the laser pulse arrives at the origin of the coordinate at time zero to make equation (S1) simpler. The origin is also on the input plane of the first diffuser slap. Then the time integrated PSF is calculated as follows.

$$PSF = \phi(x,y) = \int_0^T \phi(x,y,t)dt \qquad \text{(S2)}$$

where T is the integration time of camera.

The reduced scattering coefficient is founded as $\mu_s' = 33\ cm^{-1}$, with which, the correlation coefficients between the measured and fitted PSFs are 0.997 and 0.999 for the two diffusion slabs.

Note 2: DOP Algorithm

Our DOP algorithm is to solve the optimization (1) presented in the main text. Two constraint functions are used to control the sparsity ($C_1(O')$) and continuity ($C_2(O')$) and further enhance the reconstruction quality. The constraint functions are as follows:

$$C(O') = \lambda_1 * C_1(O') + \lambda_2 * C_2(O') \qquad \text{(S3)}$$

$$C_1(O') = \|O'\|_1 = \sum_{i,j} |O'_{i,j}| \qquad \text{(S4)}$$

$$C_2(O') = \sum_{i,j} \sqrt{\left(O'_{i+1,j} - O'_{i,j}\right)^2 + \left(O'_{i,j+1} - O'_{i,j}\right)^2} \qquad \text{(S5)}$$

where $O'_{i,j}$ refers to the pixels in the two-dimensional object.

The steepest descent algorithm was chosen for this work due to its clear theoretical basis, simple structure, low computational complexity and minimal dependence on the initial guess. The initial object estimation is assumed to be the real camera image, and it will evolve during the process of optimization, for example, at the nth iteration, the O'_n will be updated as below:

$$O'_n = O'_{n-1} - s * G_n \quad \text{(S6)}$$

Here, s denotes the step size and G_n is the gradient of the objective function mentioned in equation (1) at nth iteration.

When the diffusive material is unknown, the optimization problem (Eq. 1 in the main text) is more challenging as both PSF_1 and PSF_2 are unknown. We approximate the PSF as a two-dimensional Gaussian function with equal standard deviations ($\sigma_x = \sigma_y$). Therefore, the PSFs are now functions of their respective parameters σ_1 and σ_2, and the optimization problem becomes:

$$\underset{O', \sigma_1, \sigma_2 \in R}{minimize} \ \frac{1}{2}\Sigma_i \left|\left|[(I_i * PSF_{g1}(\sigma_1)) \odot O'] * PSF_{g2}(\sigma_2) - M_i\right|\right|_2^2 + C(O') \quad \text{(S7)}$$

In previous research, a Gaussian function can replace the PSFs because of their similarity[5]. Compared to diffusion equation approximated PSF that has 3 independent parameters to optimize (μ_a, $\mu_{s'}$ and thickness d), Gaussian PSF only has 1 parameter (σ), which makes it easier for object reconstruction with unknown materials. After this initial optimization, a narrow range of Gaussian PSFs centered around the optimal PSF is selected and considered as potential candidates for the real PSF.

The next optimization step aims to estimate better PSFs, which are the solutions of diffusion equation. i.e. diffusion-based PSF (Eq. S8), leveraging their inherent similarities with Gaussian PSFs.

$$\underset{\mu_{a1}, \mu'_{s1}, t1, \mu_{a2}, \mu'_{s2} \in R}{minimize} (2 - corr(PSF_{g1}, PSF_{d1}) - corr(PSF_{g2}, PSF_{d2})) \quad \text{(S8)}$$

After successfully estimating the diffusion parameters, it is easier to optimize the O' so that the distance between the real camera images and guessed camera images can be minimized, as shown in equation (S9):

$$\underset{O' \in R}{Minimize} \ \frac{1}{2}\Sigma_i \left|\left|[(I_i * PSF_1) \odot O'] * PSF_2 - M_i\right|\right|_2^2 + C(O') \quad \text{(S9)}$$

Finally, based on the objective value, we find the global optimization. The final image is the average of several reconstructed images around the global optimization.

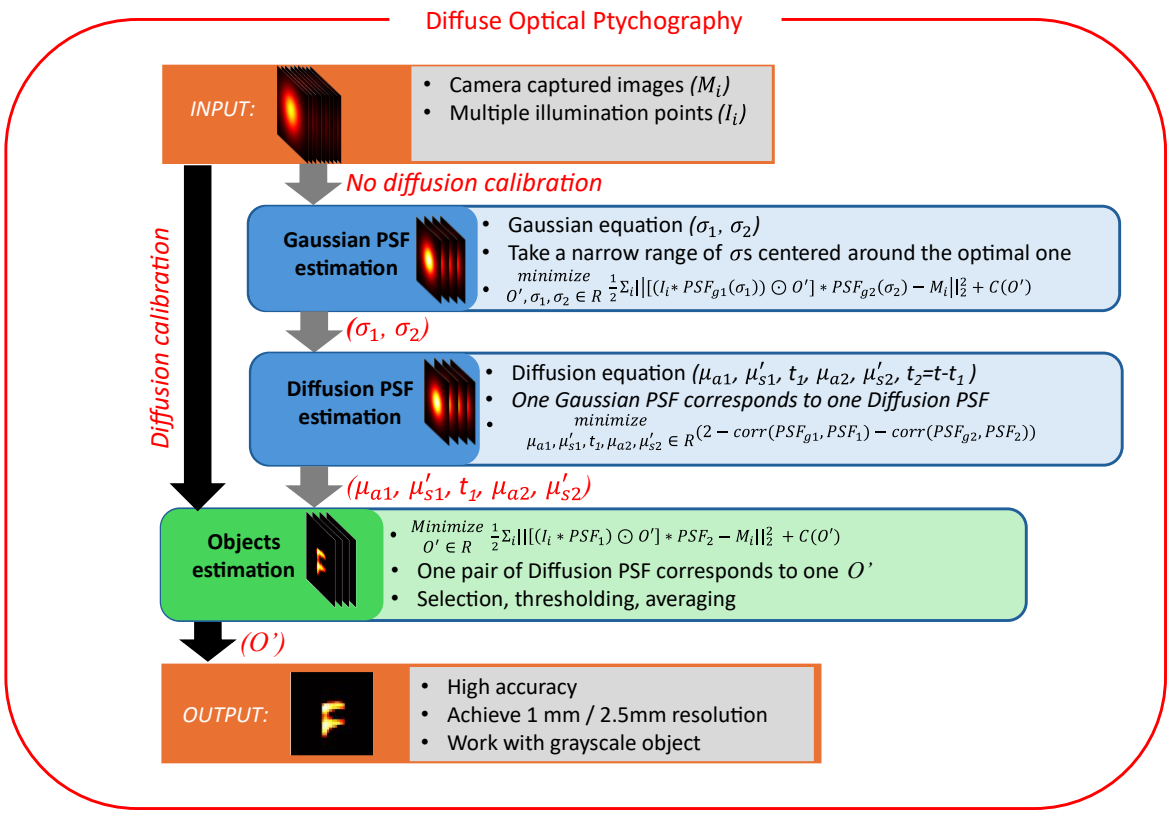

Figure S8. Flow chart for DOP, where the PSFs can be measured or estimated to reconstruct the object's image.

References:

[1]. Lyons, A., Tonolini, F., Boccolini, A. *et al.* Computational time-of-flight diffuse optical tomography. *Nat. Photonics* **13**, 575–579 (2019).

[2]. Qin, J. & Lu, R. Hyperspectral diffuse reflectance imaging for rapid, noncontact measurement of the optical properties of turbid materials. *Appl. Opt.* **45**, 8366–8373 (2006).

[3]. Wang, L. V. & Wu, H.-I. in *Biomedical Optics: Principles and Imaging* Ch. 11, 249–281 (2007).

[4]. Yoo, K., Liu, F. & Alfano, R. When does the diffusion approximation fail to describe photon transport in random media? *Phys. Rev. Lett.* **64**, 2647 (1990).

[5]. Attarwala, A. A. *et al.* A method for point spread function estimation for accurate quantitative imaging. *IEEE Trans. Nucl. Sci.* **65**, 961–969 (2018).